Chemical Physics Letters 492 (2010) 131–136

Contents lists available at ScienceDirect

Chemical Physics Letters

journal homepage: www.elsevier.com/locate/cplett

Oxygen dissociation on nitrogen-doped single wall nanotube: A first-principles study

Bin Shan [a,b,*], Kyeongjae Cho [b,c]

[a] Department of Materials Science and Engineering, Huazhong University of Science and Technology, Wuhan 430074, Hubei, China
[b] Department of Materials Science and Engineering, The University of Texas at Dallas, Richardson, TX 75080, United States
[c] Department of Physics, The University of Texas at Dallas, Richardson, TX 75080, United States

ARTICLE INFO

Article history:
Received 5 March 2010
In final form 19 April 2010
Available online 22 April 2010

ABSTRACT

Nitrogen-doped (N-doped) single wall nanotubes (SWNTs) have recently been shown to have good catalytic reactivity towards oxygen reduction reaction (ORR). We used density functional theory calculations to explore reaction paths for facile oxygen dissociation on modified SWNTs, including nitrogen doping, Stone–Wales (SW) defects, and a combination of these two. It was found that oxygen dissociation is facilitated on carbon atoms neighboring a nitrogen dopant, with the dissociation barrier reduced from 2 eV to 0.68 eV. The activation barrier can be further reduced to 0.03 eV in the vicinity of a N-doped SW defect. The reduction in barrier height is explained through the local density of states analysis.

1. Introduction

To enable a large scale utilization of fuel cells for energy-related applications, efficient and low cost electrocatalysts are highly desired. Traditionally, transition metal nanoparticles have been used as electrocatalysts to facilitate an efficient oxygen reduction reaction (ORR). However, these metals and alloys are quite rare and expensive. Over the past years, much research efforts have been devoted to enable metal-free active sites for electrochemical reduction of oxygen molecules. Nanostructures such as single wall nanotubes (SWNTs) hold great potential for such applications. SWNTs exhibit extraordinary physical and chemical properties, such as superior structural stability and mechanical strength [1], huge surface area [2], and enhanced thermal conductivity [3]. Though undoped SWNTs are quite inert towards ORR, their chemical properties can be easily tuned by chemisorption [4] or substitutional doping [5–9]. Nitrogen doping of SWNT has been extensively explored because the interaction between the lone-pair electrons from nitrogen dopant and the carbon π-electron may dramatically influence the electronic and chemical properties of nanotubes [10–13]. It has been theoretically predicted that substitutional doping of SWNTs by nitrogen can lead to modified electronic and chemical properties as well as their interactions with gas molecules or ions [5,7–9,13]. Simulations show that nitrogen doping of SWNT lead to enhanced dissociative adsorption of hydrogen for hydrogen storage applications [14]. Recently, facile ORR has been observed experimentally in metal-free Nitrogen-doped (N-doped) nanotubes, carbon nanotube cups, and graphene [15–17].

Efficient oxygen dissociation is crucial to the overall process of ORR. In this study, we investigate the effects of nitrogen doping and Stone–Wales (SW) defect [18] (a 5–7–7–5 topological defect formed by a single bond-rotation) on the oxygen dissociation barrier. Our calculation indicates that nitrogen doping influences the electronic structure and charge transfer capability of the neighboring carbon atoms and reduces the oxygen dissociation barrier from 2.0 eV on pure SWNT to ca. 0.68 eV on N-doped SWNT. The activation barrier can also be lowered by the introduction of a SW defect. The lowest barrier of ca. 0.03 eV can be achieved for oxygen dissociation over a N-doped SW defect. Energetics show that nitrogen atom prefer to occupy a site adjacent to, but not directly on the rotated bonds in SW defect, facilitating the almost barrierless dissociation of oxygen over the N-doped SW defect.

2. Methods

We performed first-principles density functional theory (DFT) total energy calculations using projected augmented wave method with Perdew–Burke–Ernzerhof (PBE) approximation for the exchange–correlation functional, which has been shown to give accurate results for a variety of molecular energies and structures [19]. The Vienna ab initio simulation package (VASP) was used for the calculations [20]. The Kohn–Sham single electron wavefunction was expanded by plane waves with an energy cut off of 400 eV, which was tested to give good convergence for total system energies. Six Monkhorst–Pack *k*-points [21] were sampled in the one dimensional Brillouin zone for total energy calculations. For local

* Corresponding author at: Department of Materials Science and Engineering, Huazhong University of Science and Technology, Wuhan 430074, Hubei, China
E-mail addresses: stanfordbshan@gmail.com (B. Shan), kjcho@utdallas.edu (K. Cho).

0009-2614/$ - see front matter © 2010 Elsevier B.V. All rights reserved.
doi:10.1016/j.cplett.2010.04.050

density of states calculations, we have used a denser 30 k-point mesh.

Generally speaking, the reactivity of a nanotube has a close relationship with its curvature, which has been demonstrated by the relationship between adsorption energies and the effective pyramidal angle [22]. In this report, we used a (10,0) zig-zag SWNT as a representative model to study the adsorption and dissociation of O_2 on small diameter SWNTs with nitrogen doping, on SW defect, and on N-doped SW defect. A detailed study on the curvature effects on dissociation barrier will be published elsewhere. Sufficient vacuum was included along the transverse direction. For direction along the tube axis, we used a double cell to minimize the coupling between oxygen molecules. The resulting dimension of the orthorhombic cells was $20 \times 20 \times 8.53$ Å^3. The geometry was optimized by conjugate gradient method and terminated once the Hellmann–Feynman force on each atom was less than 0.05 eV/Å. The calculations were carried out using spin polarized scheme. The binding energies of atomic and molecular oxygens on SWNTs are calculated using the following equation:

$$\Delta E_{\text{binding}} = E_{\text{total}} - E_{\text{SWNT}} - \frac{1}{2}E_{O_2}, \quad (1)$$

where E_{total}, E_{SWNT}, E_{O_2} refer to the energies of the total system, the SWNT and the oxygen molecule in its triplet ground state, respectively. By definition, $E_{\text{binding}} < 0$ corresponds to stable exothermic adsorption.

The minimum energy paths for oxygen dissociation reaction on SWNT surface and over SW defects were obtained by the nudged elastic band (NEB) method [23]. Eight intermediate images were used to interpolate the reaction path between the reactant state and product state. The total energy of the path was then minimized with atomic movements restricted to the hyperplane perpendicular to the reaction path. Once the minimum energy path was converged, the activation barrier for oxygen dissociation can be readily determined from the energy of the highest image along the path. The energy values reported are with reference to gas phase O_2.

3. Results and discussion

3.1. Oxygen adsorption and dissociation on an ideal (10,0) SWNT

We first discuss the oxygen adsorption and dissociation on an ideal (10,0) SWNT. The splitting of oxygen molecule into atomic oxygens on a SWNT surface generally takes place via two steps. The first step involves the adsorption process, during which oxygen molecule first becomes weakly bound physisorbed state, and upon further decrease in distance to the SWNT surface, transitions into chemisorbed state. In the second step, adsorbed oxygen molecule overcomes a transition state barrier and dissociates into two oxygen atoms. Since atomic oxygens are the intermediate species that is reactive towards a complete ORR, facile oxygen dissociation is crucial to the overall process of ORR [24].

For oxygen adsorption on (10,0) SWNT, we considered three possible adsorption states, as shown on the left panel of Fig. 1: above the center of the hexagonal ring (H-site), on top of the axial C–C bond (A-site), and on top of the zig-zag C–C bond (Z-site). As can be seen from Fig. 2, physisorption of oxygen molecules over these sites have an average oxygen molecule to SWNT distance (d) of around 3.0 Å and the binding is fairly weak. The binding energies as calculated by PBE functional are in the range of 0 to 20 meV. Such weak interaction between the oxygen and SWNT is characteristic of physisorption and the oxygen molecule retains its triplet state. Our result is consistent with reported equilibrium distance of 2.9 Å and a binding energy of 0.25 eV [4], considering that the local density approximation used in the previous study tends to overestimate binding energies. We note that an accurate prediction of the physisorption energy by DFT is hampered by its inability of accurately treating the intermolecular correlation [25,26]. However, since we are primarily interested in the oxygen dissociation behavior in this study, small variations in the weak physisorption energy will not change the overall picture.

Upon decreasing distance to around 1.5 Å, oxygen molecule transitions to a singlet chemisorbed state. The chemisorbed state act as the precursor state to subsequent oxygen dissociation. The chemisorption process is endothermic over A-site (1.0 eV) and Z-site (1.2 eV) on a defect-free SWNT. The calculated reaction barriers for chemisorption are 1.36 eV and 1.38 eV, respectively. The O–O bond length (d_{O-O}) is increased to 1.50 Å in the chemisorbed state from that of 1.24 Å in the physisorbed state. Upon chemisorption, the oxygen molecule also loses its magnetic moment. Compared to molecular oxygen chemisorption on transition metal surface, which usually is exothermic by as much as 0.45 eV [27], it is expected that oxygen dissociation on SWNT would have a significant barrier as opposed to barrierless dissociation on transition metal surface. No stable chemisorption state is found for oxygen over the H-site.

Having considered oxygen physisorption and chemisorption, we discuss the oxygen dissociation channels from the chemisorbed states into atomic oxygens. Oxygen dissociation is one of the key steps in ORR. In Fig. 2, we show five possible reaction channels la-

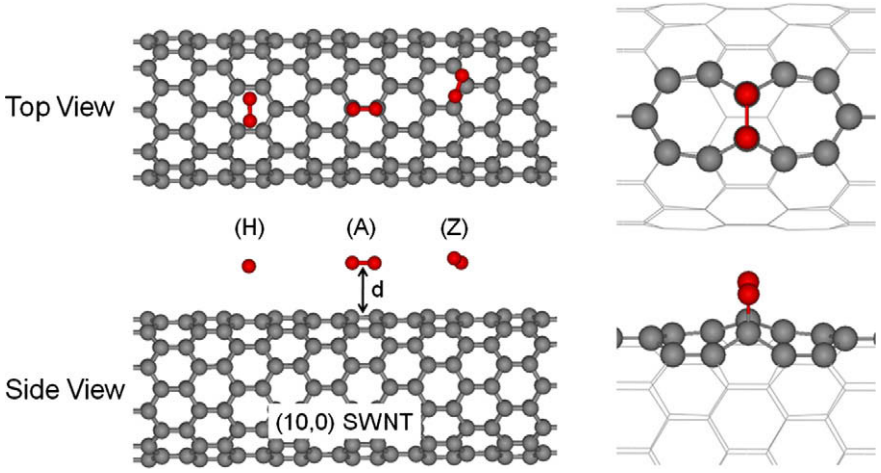

Fig. 1. Oxygen molecule adsorption configurations considered on an ideal (10,0) SWNT (left) and on SW defect (right).

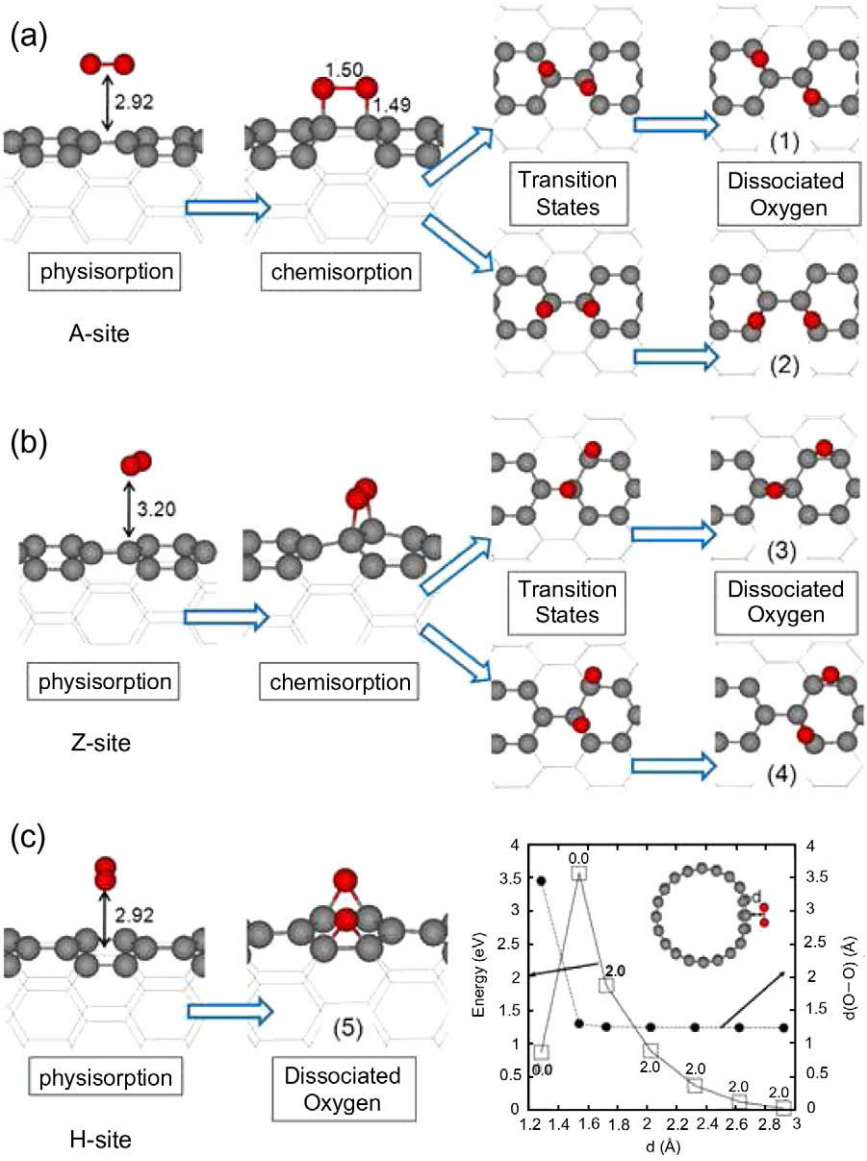

Fig. 2. Five possible oxygen dissociation channels on an ideal (10,0) SWNT starting from (a) chemisorbed state in A-site, (b) chemisorbed state in Z-site, and (c) physisorbed state in H-site. Inset in (c) shows the total energy and d_{O-O} as a function of distance between the oxygen molecule and SWNT, with numerical values on the curve indicating magnetization in units of μ_B.

beled by their final dissociated states. Channels (1) and (2) starts from A-site, (3) and (4) starts from Z-site, while channel (5) is a direct dissociation path from H-site into atomic oxygens. For dissociation channels from A-site, splitting of oxygen molecule onto different and same side of tube axis has activation barriers of 1.97 eV and 2.22 eV, respectively. For dissociations from Z-site, two reaction channels as shown in Fig. 2b are both around 2.0 eV. The dissociation of oxygen molecule starting from the H-site (channel 5) is slightly different from channels (1)–(4) in that no chemisorption state is present on the reaction path. When the oxygen molecule comes closer to the SWNT surface, it dissociates spontaneously once it crosses a high barrier of round 3.5 eV. Among all the reaction channels, the lowest barrier for oxygen dissociation on an ideal (10,0) SWNT is around 2.0 eV, which is consistent with the experimental observation that pristine SWNTs are chemically inert and do not readily activate oxygen dissociation. Detailed reaction energies and barriers, along with structural information are listed in Table 1.

3.2. Oxygen dissociation on N-doped SWNT

When a carbon atom is substituted by a nitrogen atom, the local chemical bonding environment undergoes a substantial change, which may lead to increased binding energies and more facile oxygen dissociation. We consider the electronic modifications of SWNT by the incorporation of nitrogen dopant atoms. For the study of oxygen dissociation, we contrast two cases where in one case, oxygen dissociation takes place on a site that directly involves a nitrogen dopant, while in the other case, oxygen dissociation happens on carbon sites neighboring the nitrogen dopant.

We first discuss the dissociation of oxygen over a site that has direct nitrogen participation as shown in Fig. 3a. Due to the higher electronegativity of nitrogen atom, there is a repulsive interaction between the nitrogen dopant and the O_2 molecule. This destabilizes the physisorption and chemisorption states and only one stable chemisorption state over A-site is identified. Compared to the oxygen chemisorption on pristine (10,0) SWNT, the C–O

Table 1
Energetic and structural information on the adsorption and dissociation of oxygen on (10,0) SWNT.

Reaction path		Path 1	Path 2	Path 3	Path 4	Path 5
Physisorption	Energy (eV)	0.02	0.02	0.00	0.00	0.02
	d (Å)	2.92	2.92	3.20	3.20	2.92
	d_{O-O} (Å)	1.24	1.24	1.24	1.24	1.24
Chemisorption	Energy (eV)	1.01	1.01	1.20	1.20	/
	d_{O-O} (Å)	1.50	1.50	1.51	1.51	/
	Average d_{C-O} (Å)	1.49	1.49	1.48	1.48	/
Transition state	Energy (eV)	1.97	2.22	1.94	1.96	3.55
	d_{O-O} (Å)	2.08	2.15	2.17	2.32	1.30
	Average d_{C-O} (Å)	1.42	1.41	1.41	1.40	2.00
Dissociated	Energy (eV)	0.48	0.34	0.16	0.28	0.86
	d_{O-O} (Å)	2.88	2.47	2.94	2.90	3.45
	Average d_{C-O} (Å)	1.45	1.43	1.46	1.45	1.47

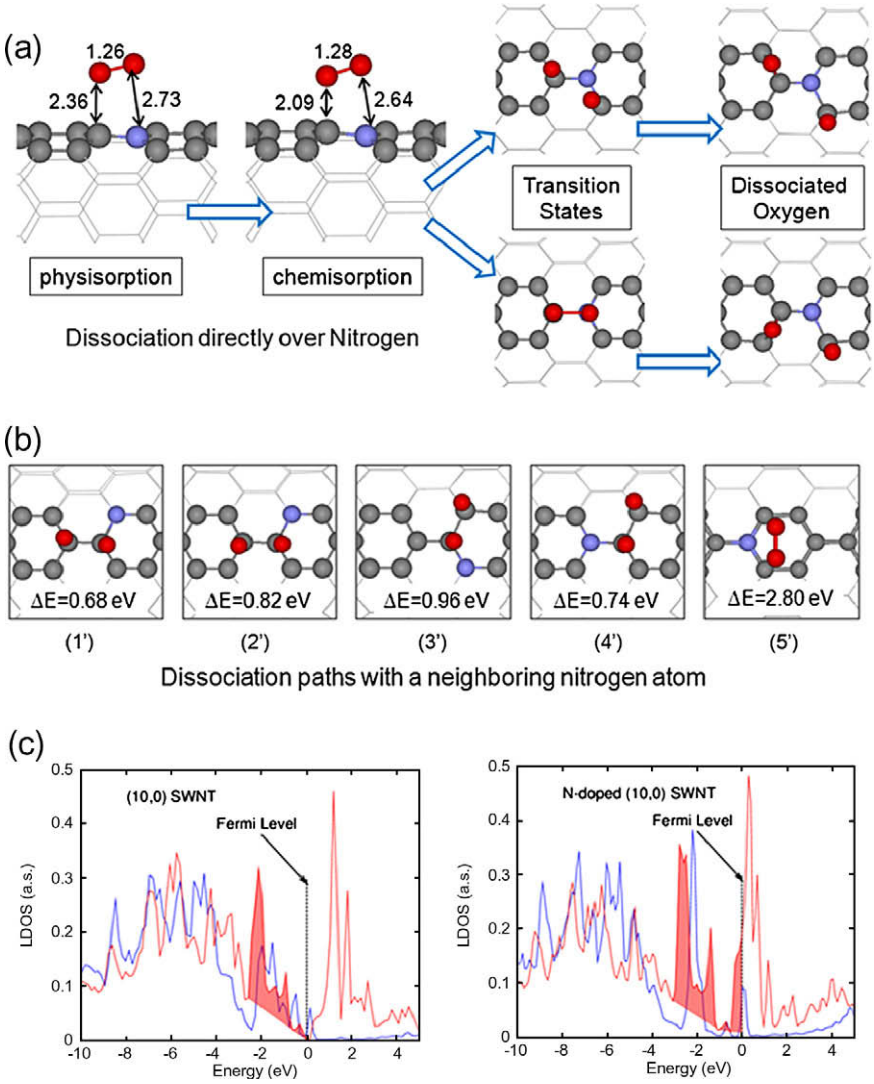

Fig. 3. (a) Dissociation of oxygen molecule directly over nitrogen substitutional site; (b) dissociation over carbon sites adjacent to nitrogen dopant, and (c) LDOS for the carbon atom involved in bonding at the transition states. The blue curves are for carbon at the transition states. The red curves are for the same C atoms in the SWNT without oxygen, with geometries fixed at the transition states. Shaded areas indicate the C($p_\perp$) LDOS that is primarily responsible for interacting with oxygen. (For interpretation of the references in colour in this figure legend, the reader is referred to the web version of this article.)

distance is significantly longer. Due to the unfavorable chemisorption configuration, the activation barrier for two possible dissociation path is 3.11 eV and 2.7 eV, respectively, much higher than the 2.0 eV barrier on a pristine SWNT. It is thus unlikely for oxygen dissociation to proceed directly over the nitrogen dopant site.

An alternative reaction path for oxygen dissociation that would have substantially different energetics is on carbon atoms that are

Table 2
Chemisorption energies, activation barriers and reaction energies of the lowest barrier path for oxygen dissociation.

	(10,0) SWNT	N-doped SWNT	(10,0) SWNT with SW defect	(10,0) SWNT with N-doped SW defect
Chemisorption energy (eV)	1.20	0.32	−0.40	−0.05
Activation barrier (eV)	1.94	0.68	0.59	0.03
Reaction energy (eV)	0.16	0.13	−3.54	−3.22

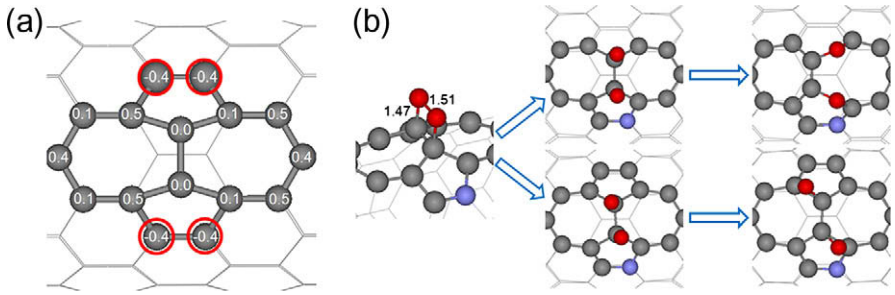

Fig. 4. (a) Stability of the nitrogen dopant in the vicinity of the SW defect. Red circle indicate the most favorable nitrogen substitution site. (b) Oxygen dissociation over most favorable N-doped SW defect carbon configuration. (For interpretation of the references in colour in this figure legend, the reader is referred to the web version of this article.)

neighboring the nitrogen dopant. In this case, the overall reaction paths are very similar to the paths (1)–(5) on a pristine (10,0) SWNT. The transition states corresponds to path (1)–(5) are shown in Fig. 3b and labeled (1′)–(5′). The heights of activation barriers for different oxygen dissociation channels are shown on the figure, indicating modified energetics and kinetics due to the presence of the neighboring nitrogen dopant. The lowest barrier (path 1′) for oxygen dissociation is around 0.68 eV, a substantial reduction from the 2.0 eV barrier on pristine SWNT. Table 2 lists the chemisorption energy, activation barrier and the reaction energy of the lowest barrier path for each case.

To gain an understanding of the reduced dissociation barrier on N-doped SWNT, we examine the electronic structures via local density of states (LDOS) analysis. We take dissociation along path (1) (Fig. 2a) as an illustrative example. LDOS on other reaction paths show similar behaviors. The left panel of Fig. 3c shows the LDOS for a carbon atom at the transition state in a pristine (10,0) SWNT. The blue and red curve represent the LDOS at transition states with and without the oxygen atoms, respectively. The part of the LDOS that lies between the Fermi level and approximately 3 eV below are the C($p_\perp$) band that participates strongly in bonding to oxygen (indicated as shaded areas in Fig. 3c) [4,14]. This band undergoes substantial change in both shape and position after interaction with oxygen. Comparing the C($p_\perp$) LDOS of a pristine SWNT to that of a N-doped one as shown in the right panel of Fig. 3c, we can see that upon nitrogen doping, there is (a) an overall magnitude increase in the C($p_\perp$) LDOS (b) a substantial increase in the LDOS at the Fermi level which are metallic electrons facilitating the chemical bond breaking reactions. Applying these observations to the barrier height analysis, we can rationalize the reduced oxygen dissociation barrier by noting that the charge transfer capability of the carbon atom neighboring a nitrogen dopant becomes larger upon nitrogen doping, which leads to an increased interaction strength at transition state and a lowered activation barrier [5]. This is also consistent with our bader charge analysis [28] that shows the electron transfer from the carbon atom to the oxygen atom at the transition state increased from 0.66 *e* to 0.76 *e* upon nitrogen doping. Similar correlations exist between the LDOS of the C($p_\perp$) band and the activation barrier of hydrogen dissociation on SWNTs [14].

3.3. Oxygen dissociation on N-doped SW defect

While we show in the previous section that incorporation of nitrogen dopant lowers the activation barrier, the lowest barrier height among different reaction channels is still 0.68 eV, a considerable barrier to overcome. To look for possibilities of further reducing the oxygen dissociation barrier, we investigate the oxygen dissociation on a SWNT with N-doped SW defect. Previous studies indicate that reactivities of gas molecules on a nanotube surface might be influenced by the presence of defect sites [29,30]. We first calculated the activation barrier on a SW defect without nitrogen doping. The configuration of the chemisorbed oxygen molecule on a SW defect is shown in Fig. 1 (right). The lowest dissociation barrier turn out to be 0.59 eV, significantly lower than the 1.94 eV on the SWNT without SW defect. The reaction path is very similar to the upper path in Fig. 4b.

When a nitrogen dopant is introduced to the vicinity of a SW defect, it is likely to segregate to an energetically favorable site. The position of the nitrogen dopant will have profound impact on the reactivity as we have shown in the previous section. A nitrogen atom sitting directly on the rotated bond of SW defect will lead to an increase in activation barrier, while a nitrogen dopant in the vicinity of the rotated bond will enhance the oxygen dissociation on the SW defect. Fig. 4a shows the energies of placing the nitrogen dopant at different substitutional sites, taking the energy of nitrogen dopant on rotated bonds as the reference. The energetically most favorable site for nitrogen doping on the SW defect is on the five-membered ring (red circles in Fig. 4a), and not directly associated with the rotated bond. This implies that nitrogen will preferentially segregate to these sites and promote the oxygen dissociation over the rotated bond on the SW defect. Transition state calculations confirm that this is the case. Fig. 4b shows two possible reaction paths for oxygen dissociation. The upper path has a barrier of 0.03 eV and the lower path has a barrier of 0.26 eV. This is the lowest barrier among the systems we investigated and the activation barrier is comparable to the barrierless oxygen dissociation on transition metal surface.

4. Conclusions

We investigated the stability and chemical reactivity of nitrogen doping and SW defect on SWNT towards oxygen dissociation. Incorporation of nitrogen dopant leads to enhanced activity on neighboring carbon atoms due to the electronic structure modification. On a SWNT with N-doped SW defect, nitrogen preferentially segregate to a five-membered ring site in the vicinity of the rotated bond and reduces the oxygen dissociation barrier to ca. 0.03 eV.

Our work clarifies the oxygen dissociation mechanism on nitrogen-doped SWNT and point towards defect engineering of N-doped SWNT for enhanced ORR.

Acknowledgements

We thank Prof. Liwei Chen at Suzhou Institute of Nano Tech and Nano Bionics for helpful discussion. The work is supported by the Program for New Century Excellent Talents in University (NCET).

References

[1] C. Wei, K. Cho, D. Srivastava, Physical Review B 67 (2003) 115407.
[2] T. Liu, T. Sreekumar, S. Kumar, R. Hauge, R. Smalley, Carbon 41 (2003) 2440.
[3] J. Hone, B. Batlogg, Z. Benes, A. Johnson, J. Fischer, Science 289 (2000) 1730.
[4] S.-H. Jhi, S.G. Louie, M.L. Cohen, Physical Review Letters 85 (2000) 1710.
[5] S. Peng, K. Cho, Nano Letters 3 (2003) 513.
[6] S. Peng, K. Cho, P. Qi, H. Dai, Chemical Physics Letters 387 (2004) 271.
[7] Z. Zhou, X. Gao, J. Yan, D. Song, M. Morinaga, Carbon 42 (2004) 2677.
[8] Z. Zhou, X. Gao, J. Yan, D. Song, Carbon 44 (2006) 939.
[9] L. Bai, Z. Zhou, Carbon 45 (2007) 2105.
[10] B.G. Sumpter et al., ACS NANO 1 (2007) 369.
[11] E. Cruz-Silva et al., ACS Nano 3 (2009) 1913.
[12] Y. Li, Z. Zhou, P. Shen, Z. Chen, ACS Nano 3 (2009) 1952.
[13] S. Yang, G.-L. Zhao, E. Khosravi, Journal of Physical Chemistry C 114 (2010) 3371.
[14] Z. Zhang, K. Cho, Physical Review B 75 (2007) 075420.
[15] K. Gong, F. Du, Z. Xia, M. Durstock, L. Dai, Science 323 (2009) 760.
[16] Y. Tang, B.L. Allen, D.R. Kauffman, A. Star, Journal of the American Chemical Society 131 (2009) 13200.
[17] L. Qu, Y. Liu, J.-B. Baek, L. Dai, ACS Nano 4 (2010) 1321.
[18] A. Hashimoto, K. Suenaga, A. Gloter, K. Urita, S. Iijima, Nature 430 (2004) 870.
[19] J.P. Perdew, K. Burke, M. Ernzerhof, Physical Review Letters 77 (1996) 3865.
[20] G. Kresse, J. Furthmuller, Computational Materials Science 6 (1996) 15.
[21] H.J. Monkhorst, J.D. Pack, Physical Review B 13 (1976) 5188.
[22] S. Park, D. Srivastava, K. Cho, Nano Letters 3 (2003) 1273.
[23] B.J. Berne, G. Ciccotti, D.F. Coker (Eds.), Classical and Quantum Dynamics in Condensed Phase Simulations, World Scientific, Singapore, 1998.
[24] J. Norskov, J. Rossmeisl, A. Logadottir, L. Lindqvist, J. Kitchin, T. Bligaard, H. Jonsson, Journal of Physical Chemistry B 108 (2004) 17886.
[25] S. Kristyan, P. Puley, Chemical Physics Letters 229 (1994) 175.
[26] T. Halgren, Journal of the American Chemical Society 114 (1992) 7827.
[27] B. Shan, N. Kapur, J. Hyun, L. Wang, J. Nicholas, K. Cho, Journal of Physical Chemistry C 113 (2009) 710.
[28] G. Henkelman, A. Arnaldsson, H. Jonsson, Computational Materials Science 36 (2006) 354.
[29] X.J. Wu, J.L. Yang, J.G. Hou, Q.S. Zhu, Journal of Chemical Physics 124 (2006) 54706.
[30] X. Lu, Z. Chen, P. Schleyer, Journal of the American Chemical Society 127 (2005) 20.